Solid Earth Discuss., 4, 889–917, 2012
www.solid-earth-discuss.net/4/889/2012/
doi:10.5194/sed-4-889-2012

Solid Earth Discussions

Insight into collision zone dynamics from topography: numerical modelling results and observations

A. D. Bottrill, J. van Hunen, and M. B. Allen

Department of Earth Sciences, Durham University, Durham, DH1 3LE, UK

Received: 28 June 2012 – Accepted: 2 July 2012 – Published: 19 July 2012

Correspondence to: A. D. Bottrill (a.d.bottrill@durham.ac.uk)

Published by Copernicus Publications on behalf of the European Geosciences Union.

Abstract

Dynamic models of subduction and continental collision are used to predict dynamic topography changes on the overriding plate. The modelling results show a distinct evolution of topography on the overriding plate, during subduction, continental collision and slab break-off. A prominent topographic feature is a temporary (few Myrs) deepening in the area of the back arc-basin after initial collision. This collisional mantle dynamic basin (CMDB) is caused by slab steepening drawing material away from the base of the overriding plate. Also during this initial collision phase, surface uplift is predicted on the overriding plate between the suture zone and the CMDB, due to the subduction of buoyant continental material and its isostatic compensation. After slab detachment, redistribution of stresses and underplating of the overriding plate causes the uplift to spread further into the overriding plate. This topographic evolution fits the stratigraphy found on the overriding plate of the Arabia-Eurasia collision zone in Iran and south east Turkey. The sedimentary record from the overriding plate contains Upper Oligocene-Lower Miocene marine carbonates deposited between terrestrial clastic sedimentary rocks, in units such as the Qom Formation and its lateral equivalents. This stratigraphy shows that during the Late Oligocene-Early Miocene the surface of the overriding plate sank below sea level before rising back above sea level, without major compressional deformation recorded in the same area. This uplift and subsidence pattern correlates well with our modelled topography changes.

1 Introduction

In this study we aim to look at the evolution through time of topography on the overriding plate at a collision zone, using 2-D numerical models of lithosphere-mantle interactions at subduction and continental collision zones. Generic modelling results are compared to specific observations from the Arabia-Eurasia collision zone. The study

SED

4, 889–917, 2012

aims to illustrate that topography can be used as an indicator of the dynamics associated with continental collision and slab break-off.

To a first order, the topography of the Earth's surface can be explained by variable crustal thickness via isostasy. However crustal thickness is just one contributor to the Earth's topography and to fully account for topography we need to consider all forces that act on the Earth's surface. The forces that influence topography can be broadly categorised into isostatic forces from thermal and crustal buoyancy, flexure forces due to elasticity associated with the lithosphere and stresses imposed at the base of lithosphere due to mantle dynamics. Topography driven by flow in the mantle is referred to as dynamic topography (Lithgow-Bertelloni and Silver, 1998). Many modelling studies have found a change in the dynamics of mantle flow during the transition between subduction, collision, and oceanic slab break-off (Gerya et al., 2004; Andrews and Billen, 2009; Duretz et al., 2011). These changes in flow in the mantle would be expected to affect the topography generated due to changes in the stresses at the base of the lithosphere (Faccenna and Becker, 2010).

Subduction zone topography is characterised by a long linear oceanic trench flanked by an outer rise on the subducting plate side and raised topography on the overriding plate (Melosh and Raefsky, 1980; Hager, 1984; Gephart, 1994). The origin of this topography is the result of the sum of dynamic forces and isostatic forces (Forte et al., 2010; Husson et al., 2011). Linking of subduction dynamics to topography (Husson, 2006) has shown how features such as the back arc basin depth can be correlated to subduction velocity. Numerical modelling (Husson, 2006) and analogue models (Husson et al., 2011) further allow predictions of topography due to mantle dynamics.

Crustal shortening and thickening at collision zones produces topographic signals, via isostasy, in addition to those caused by mantle processes. The transformation of a subduction zone to a fully formed collision zone is thought to be categorised by two important events: initial collision of the continental material and later, break-off of the subducting oceanic slab. Slab break-off has been proposed to occur when the arrival of continental material at the subduction zone slows and eventually stops subduction

SED
4, 889–917, 2012

(Davies and Blanckenburg, 1995). This resistance to continued subduction by the buoyant continental crust could then cause a build-up of stress where the oceanic material joins the continent. The slow-down of subduction is also thought to allow the subducting slab to heat up, further weakening it. A combination of the build-up in stress and thermal weakening is thought to causes the slab to neck and detach. Recent numerical modelling work (Gerya et al., 2004; Andrews and Billen, 2009; van Hunen and Allen, 2011) have shown that both the these mechanisms play important roles in the ability of slabs to detach. Estimates for the lag time of break-off after initial collision vary between 5–40 Myrs (Andrews and Billen, 2009; Gerya et al., 2004; van Hunen and Allen, 2011) and have been found to be dependent on the age and associated strength of the subducted lithosphere.

Many studies have produced numerical models of the dynamics of slab break off (Buiter et al., 2002; De Franco et al., 2008; Faccenda et al., 2009; Andrews and Billen, 2009; van Hunen and Allen, 2011). Various estimates have been made of the change in topography due to slab break- off, ranging from 1–10 km (Gerya et al., 2004; Andrews and Billen, 2009; Duretz et al., 2011) of uplift due to the loss of the slab. This large variation in estimates clearly shows the need for future work.

One of the challenges with topography is to separate the contributions to topography from different sources. This is due to collision zones producing elevated topography due to the shortening and thickening of the crust as well as up lift associated with slab break-off, plate flexure and dynamic effects from the mantle. Recent work (Duretz et al., 2011) has also highlighted that different break-off dynamics would produce different topography changes. Numerical modelling results have also been related to observation for South America (Shephard et al., 2010) showing that the modelled topography changes can be observed in real subduction settings. The study by Shephard et al. (2010) focuses on the proposed drainage reversal in South America during the opening of the south Atlantic and proposes that the subsidence and uplift patterns needed can only be explained by changes in subduction dynamics influencing the topography.

SED
4, 889–917, 2012

The Arabia-Eurasia collision zone (Fig. 1) offers an area for the study of topography changes associated with collision and slab break-off (Agard et al., 2011). Collision occurred here after the closure of the Neo-Tethys ocean basin. Collision is still active in the region with GPS measurements putting the current north-south convergence rate at $\sim 2.5\,\mathrm{cm\,yr^{-1}}$ (Sella et al., 2002). The time of initial collision is still debated, but estimates vary between > 65–5 Ma (Berberian and King, 1981; Philip et al., 1989; McQuarrie, 2003; Ghasemi and Talbot, 2006). A common estimate is late Eocene ~ 35 Ma (Vincent et al., 2007; Allen and Armstrong, 2008; Ballato et al., 2011; Mouthereau et al., 2012) based on deformation on both sides of the suture at that time, and a shut-down of arc magmatism. In this study we will use the estimate of 35 Ma for the initial collision in this region.

Slab break-off has been estimated to have occurred at 10 Ma (Ghasemi and Talbot, 2006; Omrani et al., 2008) for the Arabia-Eurasia collision giving a delay time of ~ 25 Myrs since initial collision. This estimate for the timing of slab break-off comes from observations of collisional magmatism (Omrani et al., 2008) which is used as an indicator of slab break-off. Collisional magmatism is thought to be produced by slab break-off due to the slab's decent in to the mantle drawing hot material into the mantle wedge region. There is also evidence from mantle tomography that slab break-off has occurred at the Arabia-Eurasia collision zone (Lei and Zhao, 2007) who show low velocity regions where the slab would be expected. These low velocity regions can be interpreted as areas where the slab is no longer present and has been replaced by hot mantle material. Neo-Tethys opened in the Permian (Şengör et al., 1988) making the subducted oceanic plate entering the subduction zone just before collision approximately 200 Myrs old. This old oceanic crust will have a thick lithosphere and high strength, so slab break-off would be expected to take longer than for young weak slabs. These properties support the case for using the upper estimate for the delay time between collision and break-off, of around 25 Myrs, as shown in numerical modelling studies (Andrews and Billen, 2009; van Hunen and Allen, 2011).

SED
4, 889–917, 2012

The current and past topography of the Arabia-Eurasia collision zone shows some interesting features that may allow further understanding of the dynamics of the transition from a subduction zone to a collision zone. Much of central Iran, north of the Zagros suture and within the present Turkish-Iranian plateau (Fig. 1) also has the advantage of being relatively unaffected by compressional deformation for approximately 10–15 million yr after initial collision (Ballato et al., 2011; Mouthereau et al., 2012). This means that possible dynamic mantle effects on topography are expressed without an overprint of crustal shortening and thickening. This will allow direct comparison of modelled dynamic topography with topography records from the sedimentary record in the region.

2 Methodology

The numerical modelling is done with a finite element geodynamical code, Citcom (Moresi and Gurnis, 1996; Zhong et al., 2000; van Hunen and Allen, 2011). Citcom uses a cartesian grid, assumes incompressible flow and makes the Boussinesq approximation. Non-dimensional governing equations are as follows (van Hunen and Allen, 2011):

$$\nabla \cdot \boldsymbol{u} = 0 \tag{1}$$

$$-\nabla P + \nabla \cdot (\eta(\nabla \boldsymbol{u} + \nabla^T \boldsymbol{u})) + (RaT + RbC)\hat{e}_z = 0 \tag{2}$$

$$\frac{\partial T}{\partial t} + \boldsymbol{u} \cdot \nabla T = \nabla^2 T \tag{3}$$

$$\frac{\partial C}{\partial t} + \boldsymbol{u} \cdot \nabla C = 0 \tag{4}$$

where symbols are defined in Table 1 and mantle temperature $T_m = 1350\,^\circ$C.

The code used solves for conservation of mass, momentum, energy and composition (van Hunen and Allen, 2011). The models in this study simulate the closure of a

SED
4, 889–917, 2012

small oceanic basin leading to continental collision and subsequently slab detachment. The initial model setup is shown in Fig. 2. The modelling domain is 660 km by 2640 km giving a 1 : 4 aspect ratio and boundary conditions for the model are free slip on the top and sides with no slip on the base. The thermal boundary conditions are 0 °C at the surface and mantle temperature (1350 °C) at the bottom and left edge. The right edge has a zero heat flux boundary condition. Subduction is initiated by a hanging slab and facilitated by a zone of weak material between the subducting plate and the overriding plate (Fig. 2; Appendix A). The model setup initially has a 60 Myrs old oceanic lithosphere partially subducted under a continental overriding plate. The initial thermal structure of the oceanic lithosphere is calculated using the half space cooling model. The subducting plate has a 700 km long 40 km thick continental crustal block embedded in it the lithosphere. The overriding plate also has a 40 km thick continental crust and is fixed to the right edge of the model. The thermal structure of the continental regions is set as a linear geotherm from 0 °C at the surface to mantle temperature at 150 km.

The continental material is advected using particle tracers (Di Giuseppe et al., 2008). The continental plates in the model resist subduction due their compositional buoyancy. Oceanic crustal buoyancy is ignored in the models, as the transformation of basalt to eclogite occurs at 30–40 km which would remove most additional compositional bouyancy (Cloos, 1993) making the buoyancy of the subducted oceanic lithosphere a purely thermal effect. The continental crustal thickness is initially 40 km in all continental areas of the model. The oceanic lithosphere thickness is set initially so it is proportional to its position relative to the left edge of the model. The continental lithosphere thickness is set as constant at the start of model time.

Four different deformation mechanisms are used (diffusion creep, dislocation creep, stress limiting and a model maximum viscosity). These four temperature and stress dependent deformation mechanisms are needed to accurately simulate the accepted deformation mechanisms for slabs. For a full description of rheology see van Hunen and Allen (2011).

Model topography (w) is calculated using the subaerial isostatic response from the normal stress ($q0$) at the free-slip surface. We compare cases with and without an elastic strength. For the case without any elastic strength the topography is calculated by assuming that the surface is in direct isostatic equilibrium and the normal stresses generated by the model are balanced by a column of crustal material. The height needed for this column at each nodal point in the model gives a first order estimate of the topography.

Although this does give an estimate of the topography due to both dynamic forces and the isostatic buoyancy of the material, it does not account for any elastic properties of the overriding plate. To account for the lateral elastic strength of the lithosphere the normal stress is filtered using the flexure equations for an elastic material (Turcotte and Schubert, 2002).

$$D\frac{d^4 w}{dx^4} + \nabla \rho g w = q_0(x) \tag{5}$$

where $D = \dfrac{E h_e^3}{12(1-v^2)}$

The equation is solved using a finite difference technique. The boundary conditions used in this are (1) the left edge of the model at −2.7 km to simulate the depth of the mid ocean ridge (2) the right edge is at its expected isostatic height above the mid ocean ridge (3) there is no change in topography gradient at either boundary. An effective elastic thickness (h_e) of 30 km was chosen as representative for the region based on elastic thickness estimates for the whole of Africa and the Middles East (Pérez-Gussinyé et al., 2009). We have also produced model results with 20 km, 40 km and 50 km elastic thicknesses these results can be seen in Appendix B. Results for the pre collisional back-arc depth basin depth are comparable to those by He (2012) where they use a visco-elastic numerical model of the mantle wedge and overriding plate.

SED

4, 889–917, 2012

Insight into collision zone dynamics from topography

A. D. Bottrill et al.

3 Results

This section describes how model dynamics are reflected in the surface topography and how these topographic features evolve over time.

The generally accepted process for a subduction zone becoming a collision zone is that subduction continues until continental material enters the trench, thereby slowing the subduction process (Molnar and Stock, 2009). As subduction slows, the subducted slab steepens before finally slab break-off occurs. Figure 3 shows four stages of the collision process, the resulting viscosity profile and the topographic expression. The two continental regions in the model are associated with relatively high elevations (Fig. 3a), created by the buoyancy of the continental blocks. The movement of the continental block imbedded in subducting plate can be tracked in the three further time slices in Fig. 3 from the position of crustal material. Other prominent topography features are the subduction trench and fore arc bulge, at 1700 km and 1600 km respectively.

The features that are of particular of interest are those that are on the overriding plate. This is because this area, in a collision setting, is most likely to preserve evidence of topography changes. The other reason to focus on the overriding plate is that convection in the mantle wedge is proposed to be responsible for dynamic topography. The results for this region of the model show a depression on the overriding plate at 300 km from the trench pre and post initial continental collision, but not after break-off. Before collision this feature is dynamically produced by flow in the mantle wedge (Husson, 2006). This feature is purely dynamic since the model contains no mechanism for spreading and thinning of the overriding crust. At 7 Myrs (Fig. 3b) this collisional mantle dynamic basin (CMDB) has deepened during the start of collision. At 10 Myrs (Fig. 3c) it has become shallower again, until it has almost disappeared by the time slab break-off occurs at 17 Myrs (Fig. 3d). Post collisional uplift also occurs on the overriding plate between the trench and CMDB. At 7 Myrs and 10 Myrs, this uplift is restricted to the region close to the trench where subduction of buoyant continental material is taking place. After slab break-off at 17 Myrs the uplift moves further into the overriding plate.

SED
4, 889–917, 2012

This pattern of topography change is further displayed in Fig. 4 by a topography-time map. The topography presented in the topography time map is elastically filtered with an effective elastic thickness of 30 km. This filtered topography is the same as that shown in green in Fig. 3. The Elastic filter has the effect of removing a lot of the short wavelength variation in these topographic features, and reduces the overall amplitude of the signal. Topography time plots are useful as they show which topographic features are persistent for a significant time. They also allow easy linking of the dynamics of the model to topographic changes.

Figure 4a contains three highlighted areas of particular interest. The region marked 1 shows a basin on the overriding plate, approximately 300 km back from the trench that is present between initial collision and break-off. We will refer to this post collisional basin as a collisional mantle dynamic basin (CMDB). This region is due to slab steepening as it does not correlate with subduction velocity, unlike the back arc basin feature in the same position during on-going subduction (Fig. 4a, d).

The effect of slab steepening can be more clearly observed by comparison between Fig. 3 panels (a) (5.5 Myrs), (b) (7 Myrs) and (c) (10 Myrs). These show how the slab, defined by the region of high viscosity, steepens during collision. The topography profiles for these time slices show an increase in depth of the CMDB. The steepening slab causes a deepening of the basin because it draws material away from the overriding plate causing the surface to sink. This hypothesis is further supported by the velocity fields for the three time slice in Fig. 3. At 7 Myrs the velocity field under the CMDB region has steepened to almost vertical compared to the velocity field for on-going subduction at 5.5 Myrs. At 10 Myrs the velocity field is also vertical but reduced in magnitude. This reduction magnitude of the velocity field between 7 Myrs and 10 Myrs also explains the reduction in size of the CMDB. The combined effect of slab steepening over time is shown in Fig. 4a area 1.

Region 2 in Fig. 4a marks the initial uplift after collision. This is due to the partial subduction of the continental block in the subducting plate. This creates a region with double continental buoyancy and hence of large uplift. Figure 3 shows the continental

SED
4, 889–917, 2012

material (white contour line) in the subducting plate going under the continental material on the overriding plate. This partial subduction of continental material creates areas close to the trench on the overriding plate with crustal thickness of up to 80 km.

Region 3 Fig. 4a shows migration of the uplift further into the overriding plate after slab break-off. This migration of uplift can also be seen by comparison of Fig. 3 panel (c) (10 Myrs) and (d) (17 Myrs). This change in uplift pattern in the short term is caused by the redistribution of stress after slab detachment allowing the whole region to uplift. The removal of the slab also allows some continental material to be educted back up the subduction channel as well as being underplated on to the overriding plate. The effect of this on the overriding plate is a slightly increased crustal thickness in the region due to under plating which accounts for the long term uplift seen.

To test the sensitivity of model results to various subduction model parameters a number of models calculation with different initial setups were performed. For comparison of these models the maximum depth of the post collision basin was recorded before any elastic processing had been applied. Appendix A shows how different input parameters affected the basin's depth. It was found that neither the wedge width nor viscosity affected the ultimate depth of the post collision basin by a statistically significant amount.

4 Discussion

The modelled topography evolution in this study shows a clear pattern of topography change though the processes of subduction, collision and slab break-off. Identification of these topography changes in collision zones on earth provides insight into continental collision dynamics. A schematic overview diagram of the main features of the topography change is shown in Fig. 5.

To illustrate the applicability of the presented model results, we compare them to geological observations from the Arabia-Eurasia collision zone. The Turkish-Iranian plateau is typically 1.5–2 km above sea level at present. To achieve such high topography, isostatic theory suggests the need for a large crustal thickness (Turcotte and Schubert, 2002). For example, using basic Airy isostasy to produce 3 km uplift requires a crustal thickening of ~ 33 km. Part of the crustal thickening is caused by thrusting within the crust, but active thrusting seems limited to areas with elevations below 1250 m (Nissen et al., 2011). Wholesale underthrusting/subduction of the northern side of the Arabian plate beneath Eurasia has been imaged on deep seismic lines (Paul et al. 2006), which is a plausible mechanism for generating overall crustal thickening, and hence isostatic uplift, in regions with elevation above the limit of seismogenic thrusting. Our modelling highlights the potential contribution to crustal thickening, and hence topography of such underthrusting (Fig. 4a). The spatial extent of the plateau in the model output is more localised to the overriding plate compared to the much broader uplift observed in Turkey and Iran (see region 3, Fig. 4a). This is due to the continued complete decoupling between the plates in our models after collision, whereas the coupling in a real subduction zone is likely to change throughout the subduction process.

A second topographic feature of the Arabia Eurasia collision is related to a sequence of Upper Oligocene – Lower Miocene carbonate sedimentary rocks found on the overriding Eurasian plate, in modern day Iran and southern Turkey Fig. 6 (Reuter et al., 2007). The unit is known in central Iran as the Qom Formation. The Qom Formation and its equivalents are typically 500–1000 m thick in central Iran (Gansser, 1955; Morley et al., 2009), and lie sandwiched between terrestrial clastic strata of the Lower Red Formation and the Upper Red Formation. This relationship implies that the area on the overriding plate was above sea level during the Early Oligocene, then subsided below sea level during the Late Oligocene–Early Miocene, before returning to above sea level in the late Early Miocene (Burdigalian stage). These carbonate deposits also extend laterally along most of the collision zone, suggesting that they are intimately associated with the collision process. Importantly, the carbonates indicate there was little or no compressional deformation within or adjacent to a large portion in the overriding plate in the collision zone, for up to 15 Myr after initial collision, assuming that initial collision was at 35 Ma.

SED
4, 889–917, 2012

The carbonate deposits occupy a region 200–300 km from the suture zone and have a trench-perpendicular width of approximately 200–500 km (Fig. 6) (Morley et al., 2009). The geometry and timing of the carbonate basin in Iran and Turkey (Fig. 6) fits well with the position of the distinct post initial collisional mantle dynamic basin in the modelling results (Fig. 4a, region 1). The CMDB width in our model is around 300 km (Fig. 4) this fits well with the area over which carbonate sediments are found across Iran (Fig. 6).

The CMDB is present in our modelled results for a period of 10 Myrs between collision and slab break-off. Such a pattern of topographic change fits well with the change in elevation needed to deposit the carbonate sediments that are currently found across Iran and southern Turkey. We therefore propose that slab steepening after collision (Fig. 3c) would have caused the subsidence necessary to deposit these carbonates in a CMBD.

This pattern of topography change calculated from our models is very similar to that produced in Duretz et al. (2011) but the absolute range, we found, is much closer to actual examples of subsidence or elevation seen in collision zones. This is largely a consequence of the elastic filter applied in our models. The models also reproduce well the scale of the dynamic topography modelled and observed at subduction zones by Husson (2006). Husson (2006) predicts a dynamic back arc basin of 1.5–2 km during on-going subduction similar to the models in this study before collision when subduction is at a normal rate of around 10 cm yr^{-1}.

Another geographic area that offers possibility for observation of topography change produced during continental collision is the Italian Apennines. Here, slab detachment is proposed to have started around 30 Ma and a tear propagated north to south along Italy (Wortel and Spakman, 2000). van der Meulen et al. (1999) observed a period of basin formation followed by uplift using the sedimentary record. Migrating depocentres were interpreted as evidence of a slab tear propagating north to south. Using modern estimates of the position of the suture in Italy, these depocentres seem to be mainly located on the overriding plate with the maximum observed depression around 100 km

SED
4, 889–917, 2012

from the suture. Tentatively, these observed depocentres could have been created by the same slab steepening mechanism discussed here, and be analogous to our modelled CMDB. Other authors have noted large roll back (Carminati et al., 1998; Jolivet et al., 2009) rates for subduction adjacent to Italy. This roll back would put the overriding plate into extension and could cause basin formation without the need to invoke dynamic topography. However, dating of sediments from the basins (van der Meulen et al., 1999) puts the time of deposition after initial collision, around the time of slab break-off, when the overriding plate would be expected to be in compression.

In our models there are a number of assumptions that will affect the modelled topography. One of the main assumptions is that the overriding plate doesn't shorten or thicken during subduction or collision. Substantial shortening and thickening obviously occur at collision zones, which must influence the overall topography. Our model does not allow the overriding plate to shorten and thicken, so our resultant topography does not have a component from shortening. Therefore although our study doesn't fully model the expected topography in the region it does allow us to understand the contribution of dynamic topography through time. This lack of crustal shortening and consequent crustal thickening is particularly relevant to the subduction of stretched and thinned continental material during the early stages of collision (Ballato et al., 2011).

5 Conclusions

Our modelling work emphasises that changes in surface elevation form a useful tool to study the process of continental collision. Dynamic topography is expected in the form of a back-arc basin during ongoing subduction, whose depth is correlated to subduction speed. As collision starts, this basin deepens due to the steepening of the slab. Surface uplift is expected between this basin and the trench, caused by subduction of continental material. After slab detachment, the uplift migrates into the overriding plate, where the basin had previously been.

SED
4, 889–917, 2012

These modelling results fit well with the sedimentation record and topography on the overriding plate for the Arabia-Eurasia collision zone. Upper Oligocene–Lower Miocene carbonates deposited in between terrestrial clastics show that a basin around 300 km-wide contained a shallow sea during the Upper Oligocene–Early Miocene for a period of around 8 Myr (Reuter et al., 2007). Present day high elevation of the region also fits with the expected evolution of uplift after slab break-off on the overriding plate, although there is also a contribution from internal shortening and thickening.

Appendix A

Sensitivity testing

This appendix discussed the sensitivity of modelling results to the choice of subduction model parameters. Figure A1 illustrates a suite of model runs with different input parameters. For each model the maximum depth of the back-arc depression after the onset of collision was picked in time and space. Here we can see how each input parameter has affected the depth of this depression before any elastic filtering, the value for our preferred model presented in this study is highlighted in red. All models share the initial set-up as described in the method section of this study. In Fig. A1a we show how a reduction in surface yield strength reduces the depth of the basin. This is due to a smaller surface yield strength allowing material at the boundary of the model to more easily deform and so reducing the stress at the surface used to

calculate the topography. In Fig. A1b we show how an increase in the weak zone viscosity increases the depth of the basin. In our model the weak zone viscosity defines the coupling between the subducting and overriding plate. With higher viscosity this produces greater coupling and hence a deeper basin due to slab steepening. In Fig. A1c we show how the mantle wedge viscosity has little effect on the basin depth. This is due to the basin being due to slab steepening where the majority of the stress is transmitted to the surface through the weak zone the de-couples the two plate. It

SED
4, 889–917, 2012

should be noted that the weak zone viscosity did affect the basin during ongoing subduction. In Fig. A1d we show how the width of the mantle wedge has little effect on the basin depth. This is for the same reason as the mantle wedge viscosity.

Appendix B

Elastic thickness

The effective elastic thickness h_e of the lithosphere around the Arabia-Eurasia continental collision zone is relatively poorly defined given the uncertainty in plate thickness and the effect of the suture. This appendix discusses the influence of the effective elastic thickness of the lithosphere on the topography. For a range of elastic thicknesses, greater elastic thickness give topographic features a greater lateral extent as well as reducing their magnitude. Despite quantitative differences, the discussed topographic features of this work (Fig. B1) are present over a wide range of h_e (effective elastic thickness) values, and the exact h_e value representative of the collisional tectonics settings discussed here is not the focus of this study.

Supplementary material related to this article is available online at: http://www.solid-earth-discuss.net/4/889/2012/sed-4-889-2012-supplement.pdf.

Acknowledgements. The author would like to thank his colleagues for discussions that lead to the production of this manuscript.

SED
4, 889–917, 2012

References

Agard, P. Omrani, J. Jolivet, L. Whitechurch, H. Vrielynck, B. Spakman, W. Monié, P. Meyer, B., and Wortel, R.: Zagros orogeny: a subduction-dominated process, Geol. Mag., 148, 692–725, 2011.

Allen, M. B. and Armstrong, H. A.: Arabia-Eurasia collision and the forcing of mid-Cenozoic global cooling, Palaeogeogr. Palaeocl., 265, 52–58, 2008.

Andrews, E. R. and Billen, M. I.: Rheologic controls on the dynamics of slab detachment, Tectonophysics, 464, 60–69, 2009.

Ballato, P., Uba, C. E., Landgraf, A., Strecker, M. R., Sudo, M., Stockli, D. F., Friedrich, A., and Tabatabaei, S. H.: Arabia-Eurasia continental collision: Insights from late Tertiary foreland-basin evolution in the Alborz Mountains, northern Iran, Bull. Geol. Soc. Am., 123, 106–131, 2011.

Berberian, M. and King, G. C. P.: Towards a paleogeography and tectonic evolution of Iran, Can. J. Earth Sci., 18, 210–265, 1981.

Buiter, S. J. H., Govers, R., and Wortel, R.: Two-dimensional simulations of surface deformation caused by slab detachment, Tectonophysics, 354, 195–210, 2002.

Carminati, E., Wortel, M., Spakman, W., and Sabadini, R.: The role of slab detachment processes in the opening of the western-central Mediterranean basins: some geological and geophysical evidence, Earth Planet. Sci. Lett., 160, 651–665, 1998.

Cloos, M.: Lithospheric buoyancy and collisional orogenesis: Subduction of oceanic plateaus, continental margins, island arcs, spreading ridges, and seamounts, Geol. Soc. Am. Bull., 105, 715–737, 1993.

Davies, J. and Blanckenburg, F. V.: Slab breakoff: a model of lithosphere detachment and its test in the magmatism and deformation of collisional orogens, Earth Planet. Sci. Lett., 129, 85–102, 1995.

De Franco, R., Govers, R., and Wortel, R.: Dynamics of continental collision: influence of the plate contact, Geophys. J. Int., 174, 1101–1120, 2008.

Di Giuseppe, E., van Hunen, J., Funiciello, F., Faccenna, C., and Giardini, D.: Slab stiffness control of trench motion: Insights from numerical models, Geochem. Geophy. Geosy., 9, 1–19, 2008.

Duretz, T., Gerya, T. V., and May, D. A.: Numerical modelling of spontaneous slab breakoff and subsequent topographic response, Tectonophysics, 502, 244–256, 2011.

Faccenda, M., Minelli, G., and Gerya, T. V.: Coupled and decoupled regimes of continental collision: Numerical modeling, Earth Planet. Sci. Lett., 278, 337–349, 2009.

Faccenna, C. and Becker, T. W.: Shaping mobile belts by small-scale convection, Nature, 465, 602–605, 2010.

Forte, A., Moucha, R., Simmons, N., Grand, S., and Mitrovica, J.: Deep-mantle contributions to the surface dynamics of the North American continent, Tectonophysics, 481, 3–15, 2010.

Gansser, A.: New aspects of the geology of Central Iran, Proceedings, Fourth World Petroleum Congress, Section 1/A/5, Carlo Colombo, 286–305, 1955.

Gephart, J. W.: Topography and subduction geometry in the central Andes: Clues to the mechanics of a noncollisional orogen, J. Geophys. Res., 99, 12212–12279, 1994.

Gerya, T. V., Yuen, D. A., and Maresch, W. V.: Thermomechanical modelling of slab detachment, Earth Planet. Sci. Lett., 226, 101–116, 2004.

Ghasemi, A. and Talbot, C. J.: A new tectonic scenario for the Sanandaj-SirjanZone (Iran), J. Asian Earth Sci., 26, 683–693, 2006.

Hager, B. H.: Subducted slabs and the geoid: constraints on mantle rheology and flow, J. Geophys. Res., 89, 6003–6015, 1984.

He, L.: Influence of lithosphere-asthenosphere interaction on the overriding lithosphere in a subduction zone: Numerical modeling, Geochem. Geophys. Geosy., 13, 1–13, 2012.

Husson, L.: Dynamic topography above retreating subduction zones, Geology, 34, 741–744, 2006.

Husson, L., Guillaume, B., Funiciello, F., Faccenna, C., and Royden, L. H.: Unraveling topography around subduction zones from laboratory models, Tectonophysics, 526–529, 5–15, 2011.

Jolivet, L., Faccenna, C., and Piromallo, C.: From mantle to crust: Stretching the Mediterranean, Earth Planet. Sci. Lett., 285, 198–209, 2009.

Lei, J. and Zhao, D.: Teleseismic evidence for a break-off subducting slab under Eastern Turkey, Earth Planet. Sci. Lett., 257, 14–28, 2007.

Lithgow-Bertelloni, C. and Silver, P. G.: Dynamic topography, plate driving forces and the African superswell, Nature, 395, 269–272, 1998.

McQuarrie, N.: Cenozoic evolution of Neotethys and implications for the causes of plate motions, Geophys. Res. Lett., 30, 30–33, 2003.

Melosh, H. J. and Raefsky, A.: The dynamical origin of subduction zone topography, Geophys. J. Roy. Astr. S., 60, 333–354, 1980.

SED

4, 889–917, 2012

Insight into collision zone dynamics from topography

A. D. Bottrill et al.

Molnar, P. and Stock, J. M.: Slowing of India's convergence with Eurasia since 20 Ma and its implications for Tibetan mantle dynamics, Tectonics, 28, 1–11, 2009.
Moresi, L. and Gurnis, M.: Constraints on the lateral strength of slabs from three-dimensional dynamic flow models, Earth Planet. Sci. Lett., 138, 15–28, 1996.
Morley, C. K., Kongwung, B., Julapour, A. A., Abdolghafourian, M., Hajian, M., Waples, D., Warren, J., Otterdoom, H., Srisuriyon, K., and Kazemi, H.: Structural development of a major late Cenozoic basin and transpressional belt in central Iran: The Central Basin in the Qom-Saveh area, Geosphere, 5, 325–362, 2009.
Mouthereau, F., Lacombe, O., and Vergés, J.: Building the Zagros collisional orogen: Timing, strain distribution and the dynamics of Arabia/Eurasia plate convergence, Tectonophysics, 532–535, 27–60, 2012.
National Iranian Oil Company: Geological Map of Iran Sheet 2 North-Central Iran, scale 1 : 1 000 000, Tehran: National Iranian Oil Company, 1977a.
National Iranian Oil Company: Geological Map of Iran Sheet 5 South-Central Iran, scale 1 : 1 000 000. Tehran: National Iranian Oil Company, 1977b.
National Iranian Oil Company: Geological Map of Iran Sheet 1 North-west Iran, scale 1 : 1 000 000, Tehran: National Iranian Oil Company, 1978.
Nissen, E., Tatar, M., Jackson, J. A., and Allen, M. B.: New views on earthquake faulting in the Zagros fold-and-thrust belt of Iran, Geophys. J. Int., 186, 928–944, 2011.
Omrani, J., Agard, P., Whitechurch, H., Benoit, M., Prouteau, G., and Jolivet, L.: Arc-magmatism and subduction history beneath the Zagros Mountains, Iran: A new report of adakites and geodynamic consequences, Lithos, 106, 380–398, 2008.
Paul, A., Kaviani, A., Hatzfeld, D., Vergne, J., and Mokhtari, M.: Seismological evidence for crustal-scale thrusting in the Zagros mountain belt (Iran), Geophys. J. Int., 166, 227–237, 2006.
Pérez-Gussinyé, M., Metois, M., Fernández, M., Verges, J., Fullea, J., and Lowry, A. R.: Effective elastic thickness of Africa and its relationship to other proxies for lithospheric structure and surface tectonics, Earth Planet. Sci. Lett., 287, 152–167, 2009.
Philip, H., Cisternas, A., Gvishiani, A., and Gorshkov, A.: The Caucasus: an actual example of the initial stages of continental collision, Tectonophysics, 161, 1–21, 1989.
Reuter, M., Piller, W. E., Harzhauser, M., Mandic, O., Berning, B., Rögl, F., Kroh, A., Aubry, M.-P., Wielandt-Schuster, U., and Hamedani, A.: The Oligo-Miocene Qom Formation (Iran):

SED
4, 889–917, 2012

evidence for an early Burdigalian restriction of the Tethyan Seaway and closure of its Iranian gateways, Int. J. Earth Sci., 98, 627–650, 2007.
Sella, G. F., Dixon, T. H., and Mao, A.: REVEL : A model for Recent plate velocities from space geodesy, J. Geophys. Res., 107, 2–30, 2002.
Şenel, M.: Geological map of Turkey, scale 1 : 500 000, General Directorate of Mineral Research and Exploration, Ankara, 2002.
Şengör, A. M. C., Özeren, M. S., Keskin, M., Sakýnç, M. Özbakýr, D., and Kayan, Ý.:Origin and assembly of the Tethyside orogenic collage at the expense ofGondwana Land, Earth-Sci. Rev., 90, 119–181, 1988.
Shephard, G., Müller, R. D., Liu, L., and Gurnis, M.: Miocene drainage reversal of the Amazon River driven by plate-mantle interaction, Nature Geosci., 3, 870–875, 2010.
Turcotte, D. L. and Schubert, G.: Geodynamics, 2nd Edn., Cambridge University Press, 2002.
van der Meulen, M. J., Kouwenhoven, T., der, G. V., Meulenkamp, J. E., and Wortel, R.: Late Miocene uplift in the Romagnan Apennines and the detachment of subducted lithosphere, Tectonophysics, 315, 319–335, 1999.
van Hunen, J. and Allen, M. B.: Continental collision and slab break-off: A comparison of 3-D numerical models with observations, Earth Planet. Sci. Lett., 302, 27–37, 2011.
Vincent, S. J., Morton, A. C., Carter, A., Gibbs, S., and Barabadze, T. G.: Oligocene uplift of the Western Greater Caucasus: an effect of initial Arabia? Eurasia collision, Terra Nova, 19, 160–166, 2007.
Wortel, M. and Spakman, W.: Subduction and slab detachment in the Mediterranean-Carpathian region, Science, 291, 1910–1917, 2000.
Zhong, S., Zuber, M. T., Moresi, L., and Gurnis, M.: Role of temperature-dependent viscosity and surface plates in spherical shell models of mantle convection, J. Geophys. Res., 105, 11063–11082, 2000.

SED
4, 889–917, 2012

Table 1. Notation and symbol definitions.

Symbol	Definition	Value and units
	Non-dimensional stokes equations parameters	
T	Temperature	[°C]
$\boldsymbol{u}$	Velocity	$[\mathrm{m\,s^{-1}}]$
R_a	Thermal Rayleigh number	4.4×10^6
R_b	Compositional Rayleigh number	1.7×10^7
P	Deviatoric pressure	[Pa]
$\hat{e}_z$	Vertical unit vector	[–]
t	time	[s]
C	Composition	
T_m	Mantle temperature	1350 [°C]
	Elastic equations parameters	
E	Young's modulus	7×10^{10} [Pa]
D	Flexural rigidity	Equation 5
h_e	Elastic thickness	30000 [m]
ν	Poison's ratio	0.25
w	Deflection of the elastic beam (topography)	[m]
q_0	Normal stress	$[\mathrm{Nm^{-2}}]$
$\Delta\rho$	Density contrast between mantle and crust	660 $[\mathrm{kg\,m^{-3}}]$
dx	Model Discretisation in x direction	[m]
g	Acceleration due to gravity	9.81 $[\mathrm{ms^{-2}}]$

SED
4, 889–917, 2012

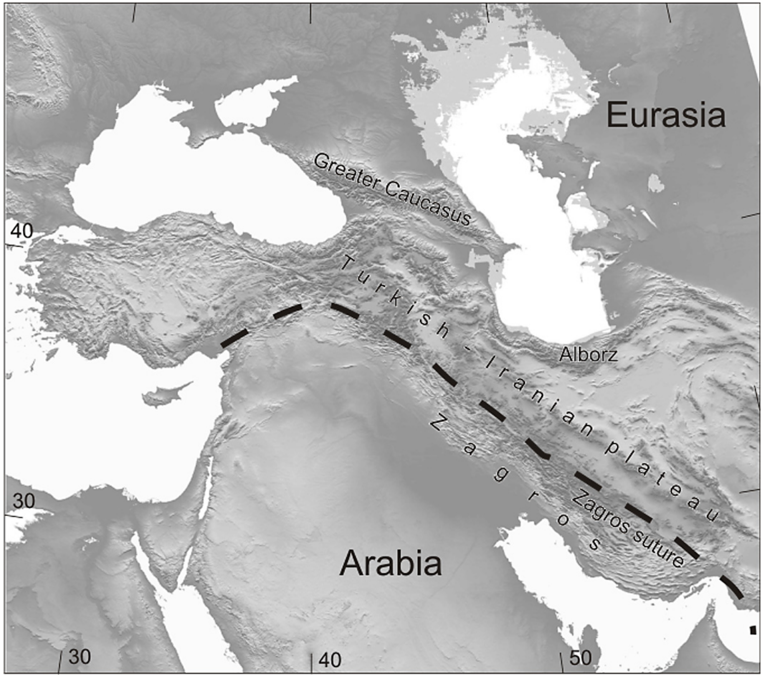

Fig. 1. Location map of the Arabia-Eurasia collision zone. The dashed line shows the position of the suture between the overriding Eurasian plate in the north and the subducted Arabian plate in the south.

SED
4, 889–917, 2012

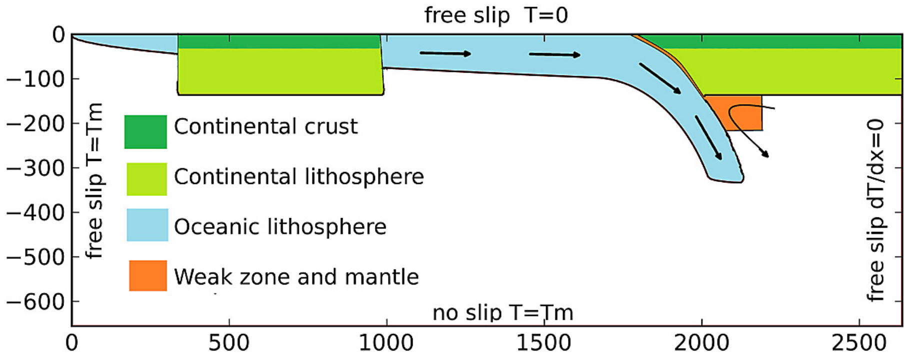

Fig. 2. The initial model setup shows the overriding plate made up of continental lithosphere and the subducting plate with a continental block embedded in oceanic lithosphere. Subduction is initiated by a pre-existing oceanic slab in a partially subducted position. Subduction is facilitated by a weak zone that decouples the subducting and overriding plates.

SED
4, 889–917, 2012

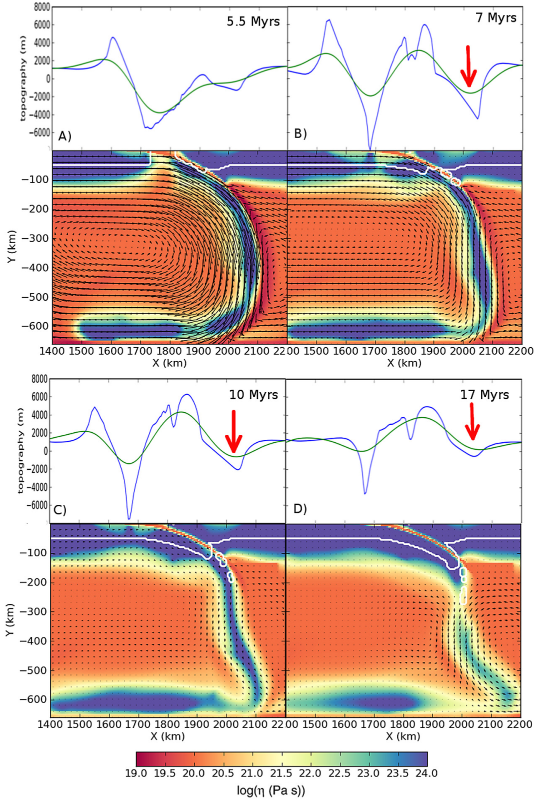

Fig. 3. Evolution of the continental collision process **(A)** before collision **(B)** at initial collision **(C)** during ongoing collision and **(D)** during slab break-off. Colour plots show the viscosity structure of the slab; white contour indicates the position of crustal material in the model, and arrows in the plot show the velocity field. Thick red arrows mark the position of the collisional mantle dynamic basin (CMDB). Line plots show topography generated by the model: blue shows the isostatic results, and green shows the effect of an elastically strong lithosphere with an effective elastic thickness of 30 km.

SED
4, 889–917, 2012

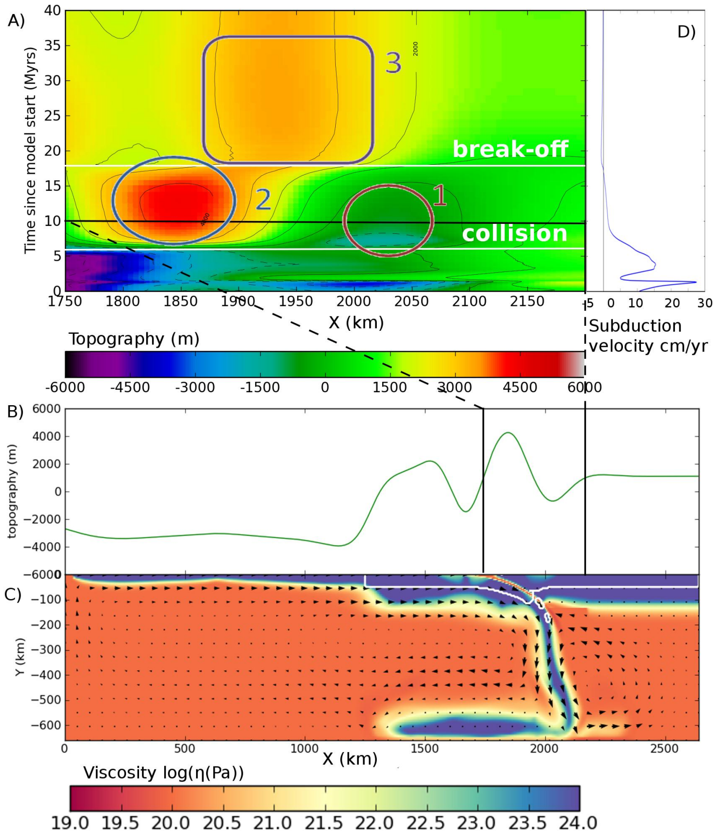

Fig. 4. (A) Topography time map (Faccenda et al., 2009; Duretz et al., 2011) showing a section of the overriding plate with the trench at the left edge of the figure. The topography is represented by the colour scale with time on the Y axis and distance on the X axis. **(B)** The topography at 10 Myrs during the collisional stage **(C)** The corresponding viscosity distribution in the model. **(D)** The subduction velocity throughout model time.

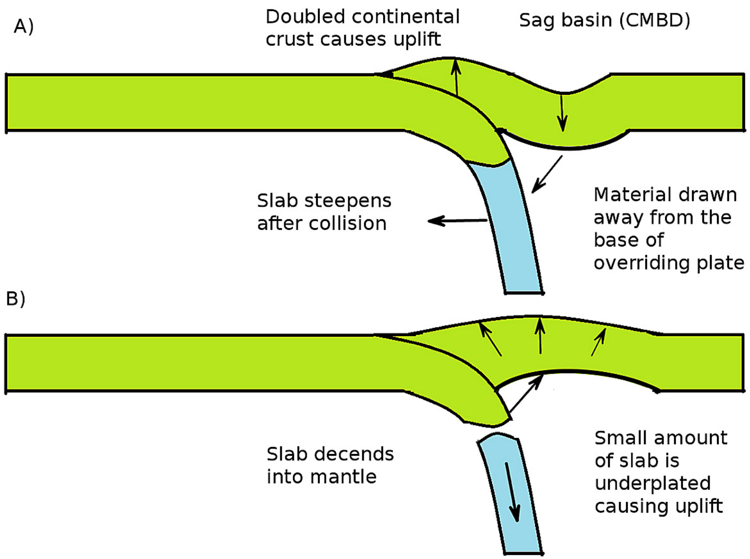

Fig. 5. Schematic diagram showing the topography evolution of the overriding plate from initial collision to slab break-off. **(A)** During initial collision uplift is generated close to the trench by under thrusting of continental material. Simultaneously, on the overriding plate a dynamic depression occurs due to slab steepening inducing flow that draws material away from the base of the overriding plate. **(B)** After slab break-off, the basin is replaced by uplift when the remains of the subducted continental block rise buoyantly under the overriding plate.

SED
4, 889–917, 2012

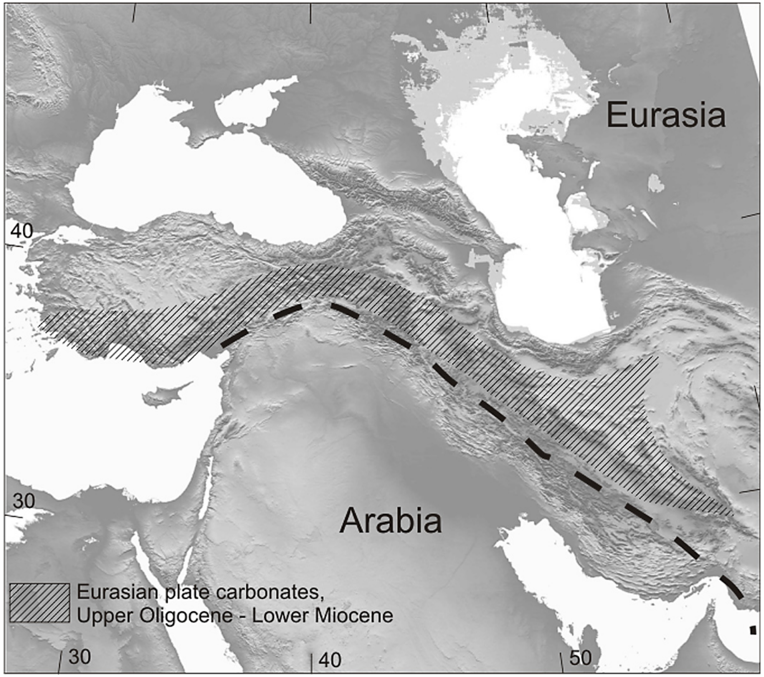

Fig. 6. The extent of Upper Oligocene–Lower Miocene carbonate strata present on the overriding Eurasian plate in the Arabia-Eurasia collision zone. These carbonate deposits were laid down after initial collision. (Compiled from National Iranian Oil Company, 1977a; National Iranian Oil Company, 1977b; National Iranian Oil Company, 1978; Şenel, 2002; Reuter et al., 2007; Morley et al., 2009).

SED
4, 889–917, 2012

Insight into collision zone dynamics from topography

A. D. Bottrill et al.

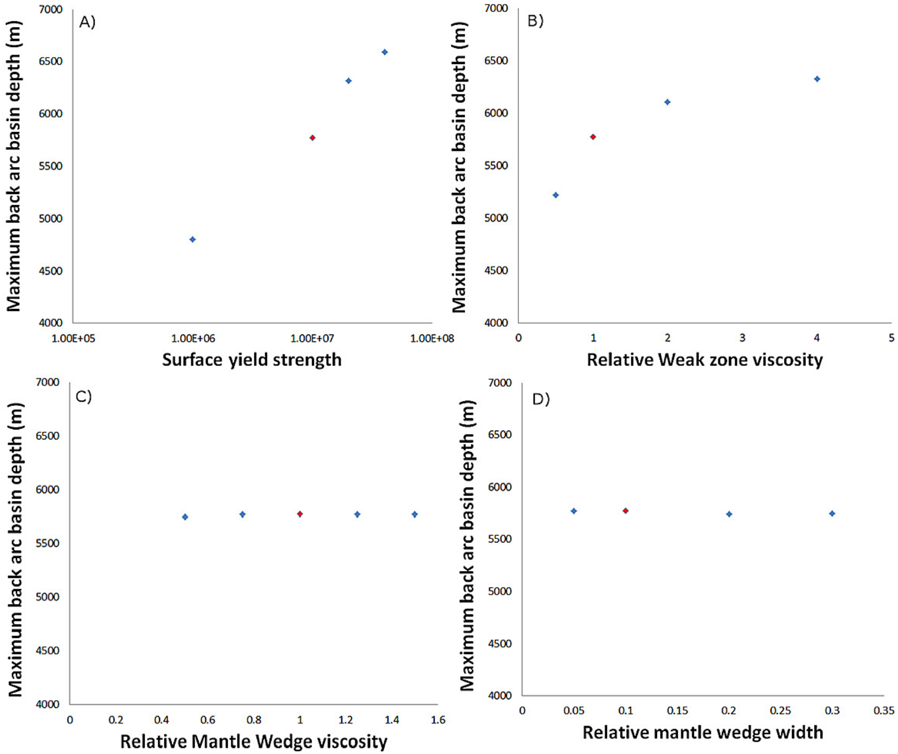

Fig. A1. Graphs showing the sensitivity of the back arc basin depth before elastic filtering to four different model input parameters.

SED
4, 889–917, 2012

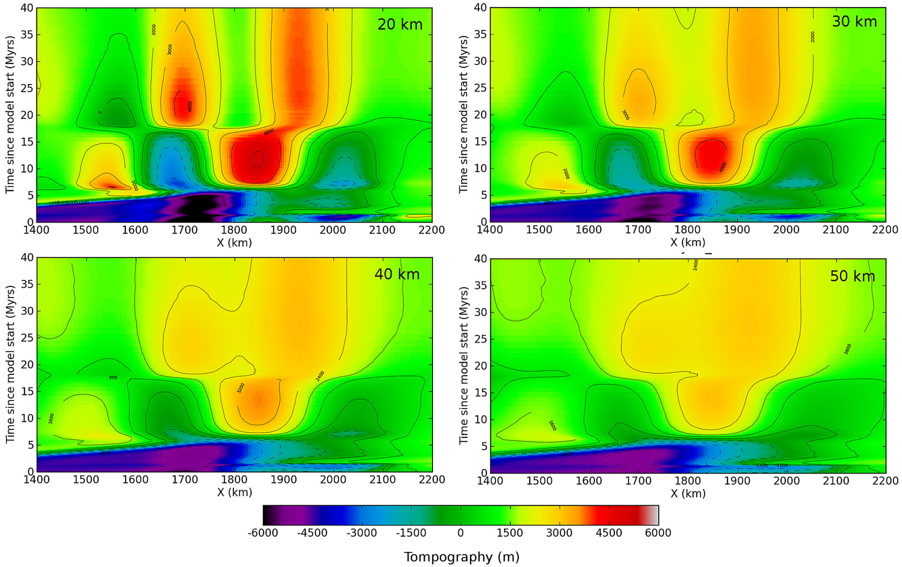

Fig. B1. Topography time maps for our results with a 20 km, 30 km, 40 km and 50 km elastic filter applied.

SED

4, 889–917, 2012

Insight into collision zone dynamics from topography

A. D. Bottrill et al.